DEM element modelling of silent piling group installation for offshore wind turbine foundations

Cerfontaine, Benjamin; Brown, Michael; Ciantia, Matteo; Huisman, Marco; Ottolini, Marius

Publication date:
2021

Document Version
Peer reviewed version

Author Accepted Manuscript: Cerfontaine, B, Brown, M, Ciantia, M, Huisman, M & Ottolini, M 2021, 'DEM element modelling of silent piling group installation for offshore wind turbine foundations', Paper presented at Second International Conference on Press-in Engineering, Kochi, Japan, 19/06/21 - 20/06/21 pp. 227.https://icpe-ipa.org/

Discrete Element Modelling of silent piling group installation for offshore wind turbine foundations

B. Cerfontaine
University of Southampton, Southampton, United Kingdom

M. Brown & M. Ciantia
University of Dundee, Dundee, United Kingdom

M. Huisman & M. Ottolini
Heerema Marine Contractors, Leiden, the Netherlands

ABSTRACT: Offshore wind farms are now built in deeper water and bigger foundations are required to stabilise wind turbines of increasing sizes. Pile driving is the most widespread foundation installation method, but more stringent environmental regulations necessitate costly mitigation methods to reduce underwater noise emis-sions. The silent piling (push-in) concept presented in this work is composed of a cluster of four piles, progres-sively installed by successive jacking sequences. During one sequence, each pile is moved downward by 0.5m stroke, while the other piles are used as reaction. This paper presents the results of Discrete Element Method (DEM) of the installation process. This work identifies the main features of the push-in installation method, such as pile interaction, progressive plugging and loss of efficiency as a function of depth. It is shown that the cluster capacity can reach six times the weight of the tool necessary to silently install the piles.

1 INTRODUCTION

Pile driving is one of the main offshore installation methods for large monopiles or smaller piles supporting the corner of jacket structures. One of the disadvantages of this method is the large amount of underwater noise generated by the repeated impact of the hammer on the pile, which can be harmful for marine inhabitants (Bailey *et al.*, 2010). Mitigation methods such as bubble curtains (Koschinski & Lüdemann, 2013), can be very expensive with an important-carbon footprint. Subsequently, there is a need for innovative and silent piling installation methods.

Pile jacking generates very low noise during installation, as it does not require impact. However, large reaction force is necessary to install a pile to a target

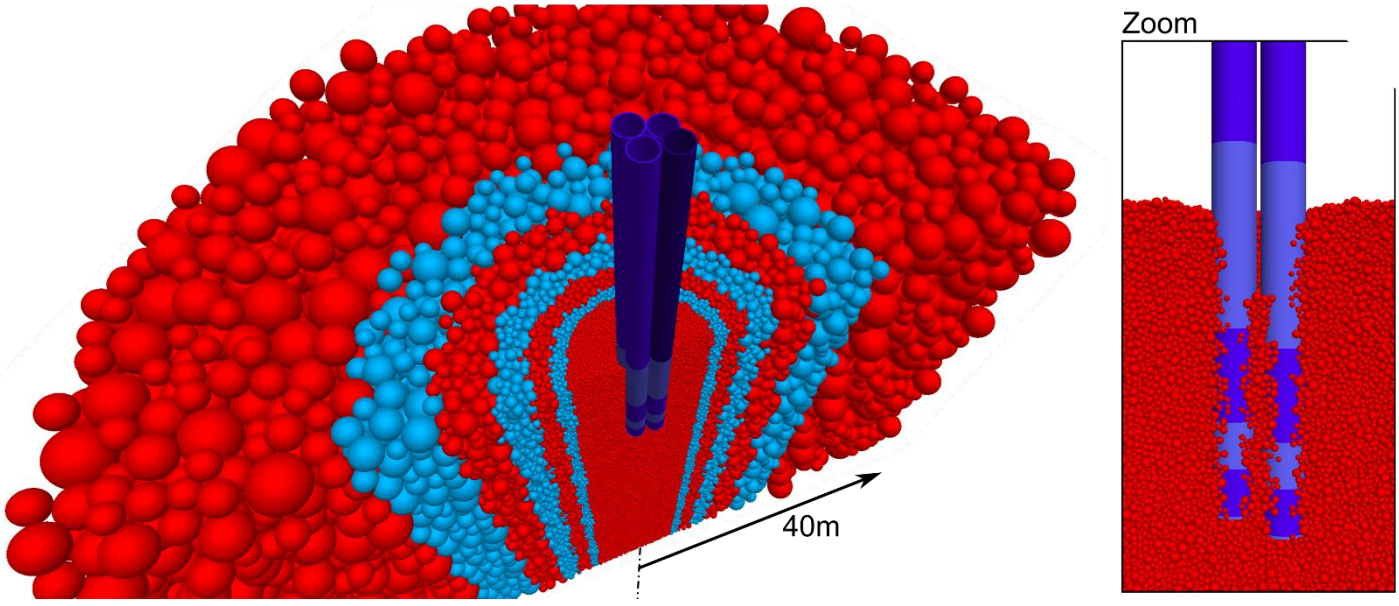

Figure 1 Half of the DEM sample, together with the four piles during installation (looking down from above)

depth. The press-in piling method overcomes this hurdle by using previously installed piles as reaction piles (White *et al.*, 2002) to create a retaining wall made of piles. The push-in concept presented here follows the same rationale. This concept replaces a traditional single open tubular pile with a cluster of four smaller diameter open tubular piles (Koschinski & Lüdemann, 2020), see Figure *1*. In a number of strokes, each of the piles in this cluster is statically pushed into the soil, with two or three piles of the cluster providing the uplift resistance required to push in a third pile, with a tool gripping on the "uplift" piles and pushing down onto the pile that is penetrating. By sequentially pushing in each of the piles while holding on to two or three others, the cluster as a whole is penetrated into the seabed. A novelty in the push-in pile concept is that the installation method makes use of force equilibrium (uplift loads equal compression loads) without moment equilibrium (one side of the cluster is pushed down with more force than the opposite side). The moment equilibrium is therefore reached by introducing bending into the piles, something that the installation tool is specifically designed for.

The Discrete Element Method (DEM) represents the soil as an assembly of rigid particles that obey Newton's laws of motion and interact between each other by means of contact laws (O'Sullivan, 2011). The DEM is often employed to investigate soil behaviour at the element scale as it offers readily accessible information at the micro-scale, which may be used to uncover relevant micromechanics.

One of the main advantages of the DEM is to easily handle large displacement and large deformation problems. For this reason Arroyo *et al.*, (2011) started to use DEM to simulate CPT in calibration chambers. Ciantia *et al.* (2016) extended this approach to investigate crushing effects on CPT and pile jacking respectively. Sharif *et al.* (2020) demonstrated the efficiency or rotary installation of piles to reduce the necessary crowd force by using DEM as a virtual centrifuge. Liu *et al.* (2019) simulated jacked open-ended piles in 2D. They showed that the plugging mechanism was related to some particle arching inside the pile. The closed-ended pile penetration mechanism was also investigated by Zhang and Wang (2015) in 3D.

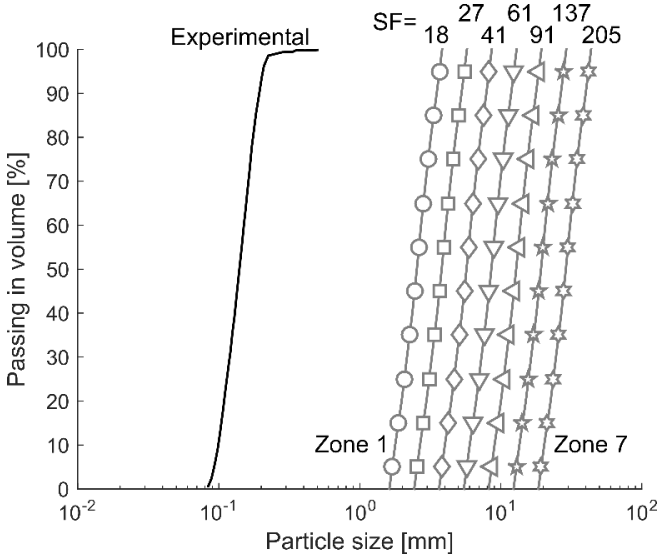

Figure 2 Comparison between experimental (from Lauder (2010) and scaled up (SF = scaling factor) particle size distributions

This paper uses the DEM to simulate the push-in installation of a four pile cluster in a sandy material. The main objective is to demonstrate the feasibility of the technique and to investigate the main physical mechanisms during installation. The problem was first simplified as a displacement-controlled installation, to understand the interaction between the piles of the cluster. A force-controlled installation, more representative of the field installation, was finally simulated. All the numerical models described here were built using the PFC3D code (Itasca Consulting Group, 2019).

2 METHODOLODY

2.1 *Preparation of the DEM sample*

The DEM framework is used to create a virtual centrifuge environment with an enhanced constant gravity field (Ng = 60), in order to simulate small-scale model and compare the results with actual centrifuge tests in the future. The sample is composed of sand particles only and represents a dry sand bed. However, it is possible to calculate an equivalent gravity scaling factor in saturated sand, i.e. the gravity scaling that would create the same initial stress distribution, assuming that the sand behaviour is drained throughout the simulation (Li *et al.*, 2010).

$$G_{sat} = \frac{\rho_d}{\rho'} G_d \tag{1}$$

where G_d (=Ng = 60 here) is the acceleration applied to a dry sample and G_{sat} (= 100) is the equivalent acceleration that would be applied to a saturated sample. The dry and buoyant densities are ρ_d and ρ' respectively. Therefore, the prototype piles in an offshore environment are scaled to 1:100. Dimensions are given at prototype scale in the following.

The sample was prepared according to the methodology detailed in (Ciantia *et al.*, 2018). A representative elementary volume (REV) is first prepared. It consists of a cylindrical slice, whose diameter is equal to the sample diameter, but whose height is one fourth of the sample height. The sample outer diameter is equal to 40m at prototype scale, and its height is equal to 60m.

A polydisperse assembly of particles is adopted here to realistically represent the HST95 sand, characterised by Lauder, (2010). Representing the sand particles at their true scale would lead to samples

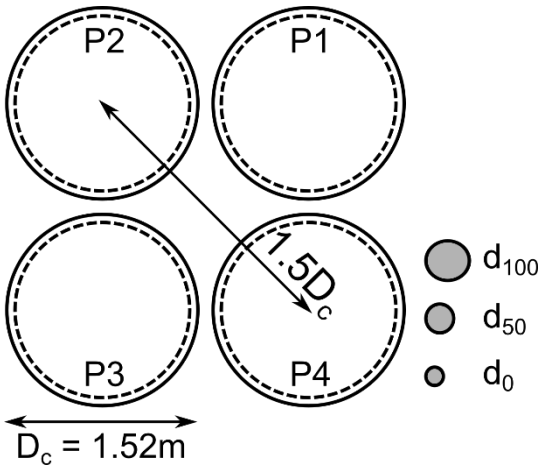

Figure 3 Cluster arrangement and comparison with the particle diameter in the core section

composed of millions of particles, which are far too computationally expensive. Therefore, the particle size distribution (PSD) was discretised into ten bins, each representing 10% of the total solid volume. Each marker in Figure *2* represents the particle diameter of one bin. A scaling factor (SF) was applied to the PSD to reduce the number of particles. The same SF is applied to all particles of the PSD, therefore the shape of the PSD is maintained, but it is shifted in size, as shown in Figure *2*. The homogeneous upscaling of all particles ensures that the soil mass behaviour is the same whatever the SF, providing there are enough particles to form a REV. Such an upscaling is quite common for DEM simulations (Evans & Valdes, 2011; Ciantia *et al.*, 2019b; Zhang *et al.*, 2019).

The REV is composed of seven zones extending radially (Figure *1*) populated with PSD affected by increasing scaling factors, ranging from 18 (centre) to 205, as shown in Figure *2*). This gradation in particle size is similar to mesh refinement in the finite element method, using smaller particles where soil-structure interaction occurs, while the far field can be modelled by larger particles. For the smallest particles, the shaft diameter (D_c) to average particle (d_{50}) ratio equal to 6. This number is greater than what is usually used in the literature for pile penetration such as CPTs (Ciantia *et al.*, 2019b). The diameter of the central zone (zone 1) is equal to 5.3m.

The particles were randomly generated within each zone of the REV to achieve a target relative density (on average 54% in central core). Such a process creates large contact forces and velocities within the sample. Therefore, a dissipation phase takes place (Khoubani & Evans, 2018), during which the kinetic energy of particles is zeroed every few time steps and large local damping is applied to the particles (0.7).

Once the system has reached a static equilibrium, four REV are stacked to create the final sample. The gravity is set up to 60g and the target stress state (K_0 = 0.47) is achieved within the sample.

Table 1 HST95 sand properties and DEM parameters

Sand properties [unit]	Symbol	Value
Minimum void ratio [-]	e_{min}	0.467
Maximum void ratio [-]	e_{max}	0.769
Critical state friction angle [°]	ϕ	32
Sand-steel friction coefficient [°]	δ	0.445
Particle dimension [mm]	d_{10}	0.09
Particle dimension [mm]	d_{50}	0.141
Particle dimension [mm]	d_{100}	0.213
Particle density [kg/m³]	ρ_s	2650
Dry density [kg/m³]	ρ_d	1637
Buoyant density [kg/m³]	ρ'	992
Coefficient of earth pressure at rest	K_0	0.47
DEM properties [unit]		
Particle shear modulus [GPa]	G	3
Particle Poison's ratio [-]	ν	0.3
Particle friction coefficient [-]	μ	0.264

The physical properties of the HST95 are given in Table *1*, together with the properties of the Hertz-Mindlin contact model adopted for the particles. The DEM parameters were obtained by back-calculation of triaxial tests (Sharif *et al.*, 2020). The average relative density in the central core of the model is equal to 54%. Particles are free to move in translation, but their rotation was fixed. This is commonly used to simulate the additional restraint of non-spherical particles (Ciantia *et al.*, 2019a) in order to capture the macroscopic response of the soil.

2.2 *Pile model and loading*

A cluster of four 1.52m (60") core diameter (D_c) piles is simulated in this work. The spacing of the piles is equal to 1.5 pile diameter from centre to centre, as shown in Figure *3***Error! Reference source not found.**. The pile wall thickness is equal to (2.5") 63.5mm. Each pile is modelled as a rigid body and split into several parts (base and five shaft segments) to identify the different contribution to the penetration resistance. The steel to particle coefficient of friction is equal to 0.4.

The pile penetration must remain quasi-static during the installation. Therefore, the DEM simulation must limit the inertial effects. The inertial number (I) is typically estimated and must be maintained below a certain threshold to ensure the simulation is quasi-static. The adopted threshold varies between 10^{-3} (Khoubani & Evans, 2018) to 10^{-2} (Janda & Ooi, 2016; Ciantia *et al.*, 2019b), although recent work has shown that lower values could be necessary for polydisperse particle distribution (Shire *et al.*, 2020). In this work, the maximum pile velocity ($v_{z,max}$) when the pile tip is at a certain depth is calculated based on the approach of (Sharif *et al.*, 2020)

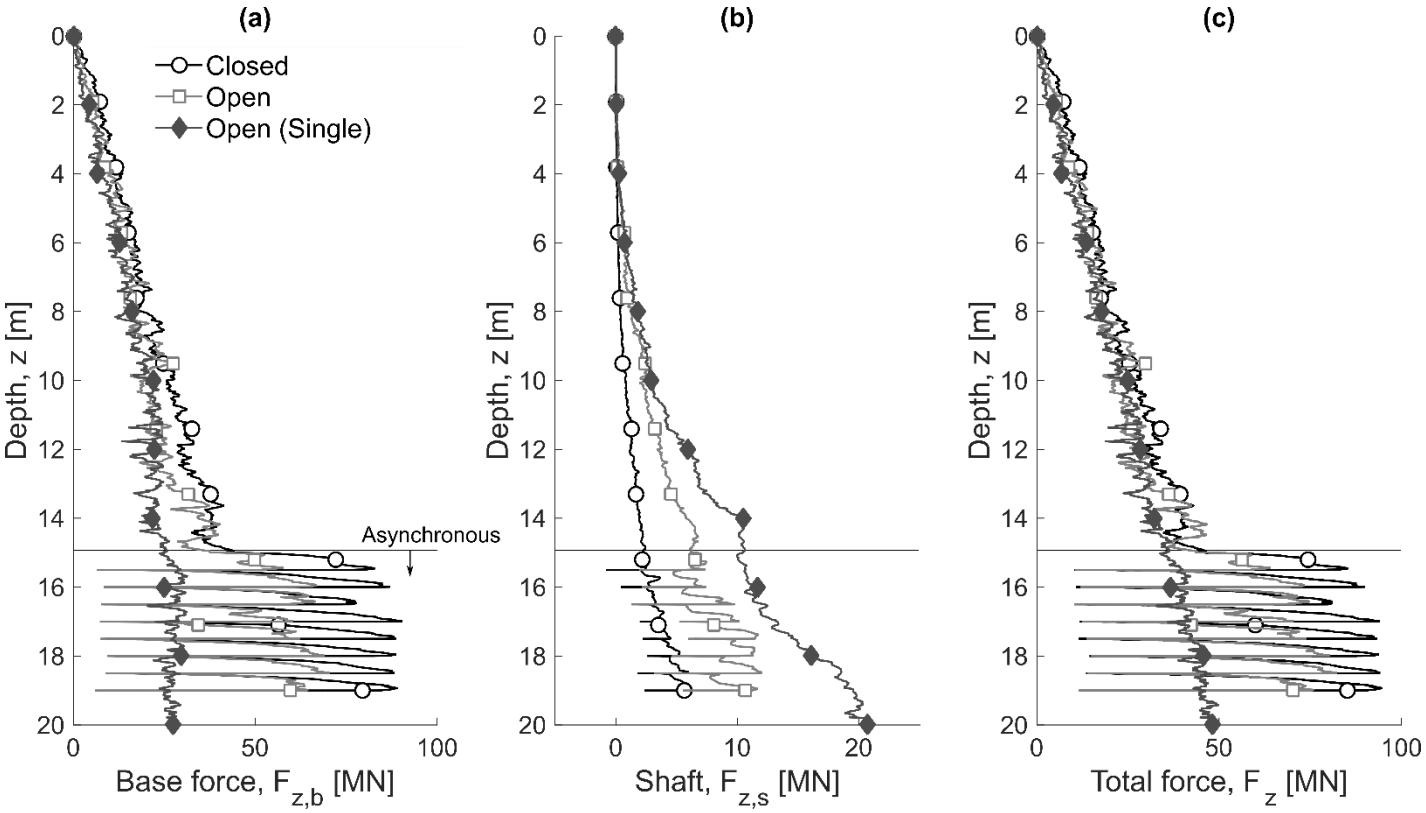

Figure 4 Comparison of the force acting on pile 1 (total, base only or shaft only) in three configurations: closed-ended pile cluster, open-ended pile cluster and single open-ended pile

$$v_{z,max} = 3D_c \frac{I}{d_{50}} \sqrt{\frac{{p_0}'}{\rho_s}} \quad (2)$$

where the inertial number I is equal to 10^{-2}, d50 is the average particle diameter of the central zone, p_0' is the initial confining pressure at the considered depth and ρ_s is the particle unit weight. The penetration rate is increased stepwise as the pile tip reaches greater depths, in order to minimise the CPU time while maintaining quasi-static conditions.

3 DISPLACEMENT-CONTROLLED

The push-in piles concept was first simplified by simulating a fully-displacement controlled installation. First, all piles were installed at the same penetration rate (synchronous phase) until 15m depth. During a second phase (asynchronous)., each pile is moved individually (0.5m stroke) while the other piles remained fixed. The cluster moves downwards by 0.5m every sequence of four steps. During the first step, pile P1 is moved downwards while piles P2, P3 and P4 are fixed. P3 is moved during step 2 (other piles are fixed), then P2 during step 3and finally P4 during step 4. The imposed displacement is represented in Figure *5*a as a function of normalised steps, one normalised step being the time necessary for one pile stroke. Several sequences were applied during the asynchronous phase until the cluster reached 19m depth.

Closed-ended and open-ended piles were tested to evaluate the effect of plugging on the installation force requirements.

3.1 *Macroscopic forces*

The macroscopic force acting on the pile base and shaft were calculated by summing the vertical component of contact forces acting on them. The shaft component include contact on the outside and the inside if the pile was open-ended. All piles of the cluster had similar behaviour, therefore only the forces acting on pile P1 are represented in Figure *4*. Results for a single open-ended pile, i.e. not part of a cluster and installed at the same position as P1, were added for comparison. Figure *4*c shows that during the synchronous installation phase (0-15m depth), the total force measured is approximately 30% greater for a closed-ended pile in the cluster than for the single pile. It is only 15% greater if the piles were open-ended. The increase in total force is due to the interaction between the piles of the cluster, while the difference between closed- and open-ended is due to the pile partial plugging, which will be discussed below. The shaft contribution is greater for open-ended piles as friction is mobilised on the inside and the outside of the pile. On the contrary, the base contribution is smaller for the open-ended piles.

The asynchronous installation of the pile starts at a depth of 15m. The measured base and total forces vary cyclically (Figure *4*) between a peak and a low value. This is one of the main features of the push-in

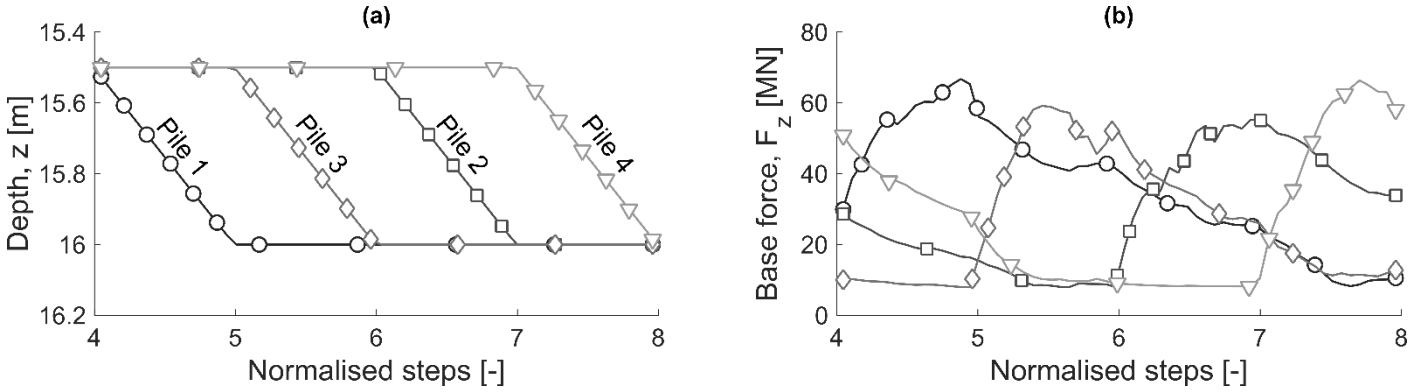

Figure 5 Zoom-in on one asynchronous installation sequence for closed-ended piles, displacement-controlled installation

process. It can be further illustrated by inspecting the evolution of the base force for each pile of the cluster during one asynchronous sequence, i.e. each pile is moved downwards of 0.5m successively (Figure *5*a). Figure *5*b shows that the base force increases for each pile when it is pushed downwards, then decreases progressively when the other piles are moved. At the end of the sequence, the force acting on each pile is different, although they have all reached the same depth.

It can be observed in both Figure *4* and Figure *5* that the force necessary during a pile stroke is approximately twice the force that was applied to the pile during the synchronous installation (phase 1, 0-15m). However, the total measured force (sum of P1 to P4) is lower than the force necessary for synchronous installation, because the compressive force decrease on all other piles. It should be noted that open-ended piles require a lower force per stroke, indicating that they are not fully plugged.

3.2 *Microscopic observations*

Figure *6* depicts a cross-section of force chains around the piles before and after pile P1 was moved downwards. At the beginning of the asynchronous sequence (Figure *6*a), the force chains are not symmetrical, which is consistent with Figure *5*b. At the end of an asynchronous sequence, the force acting on P4 is the greatest, followed by the force on P2, then P3 and P1. When P1 is moved (Figure *6*b), the force chains acting on its base increase in magnitude. Their magnitude decreases on P2, but the pile remains in compression. It can be assumed that the fixed-displacement piles adjacent to the pile being moved constrain the pile penetration failure mechanism.

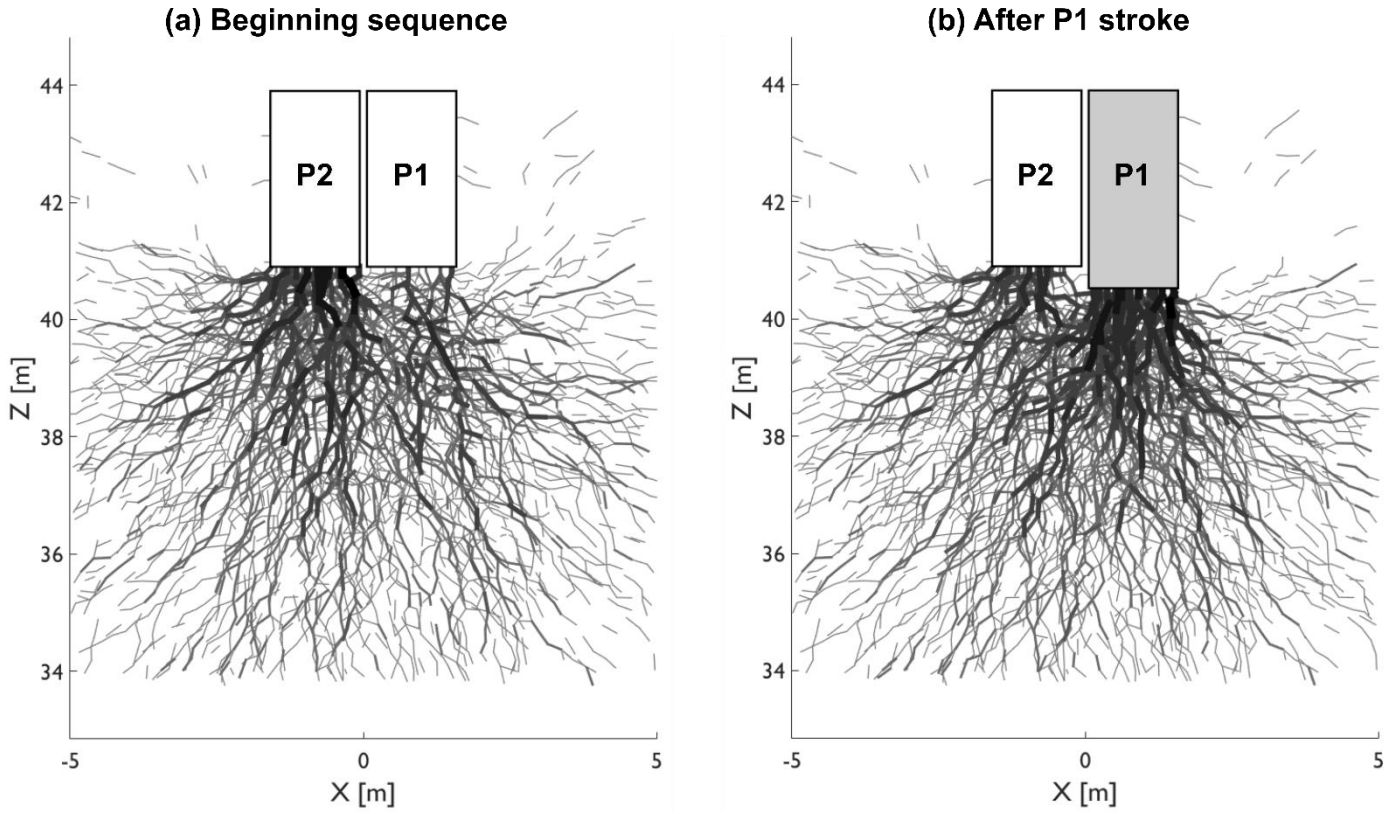

Figure 6 Force chains under the piles during the sequential installation of closed -ended piles, sequence begins at 19m depth

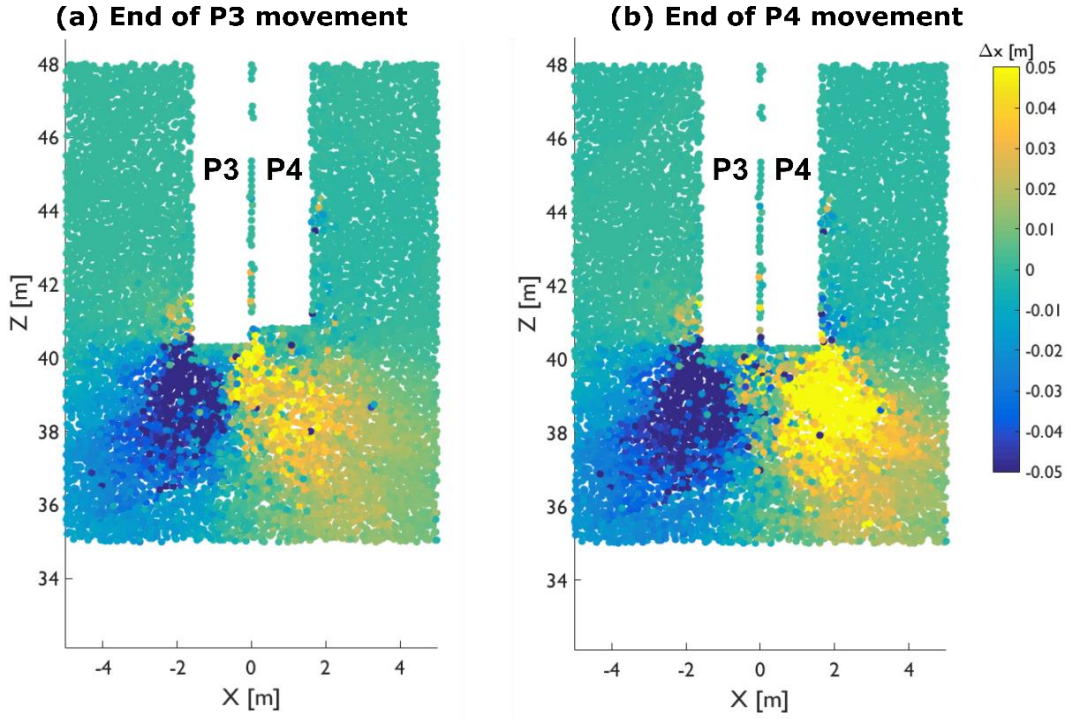

Figure 7 Horizontal displacement at the end of a sequential installation of the close-ended piles, sequence begins at 19m depth, displacement capped at +0.05 or -0.05m

Figure *7* depicts the particle displacement between the beginning (all piles at 19m depth) and the end of the asynchronous sequence (all piles at 19.5m). Each dot in the figure represents a particle, irrespectively of its diameter. The comparison of Figure *7*a and Figure *7*b shows that the installation of pile P4 mainly induced a displacement of the particles to the right (positive displacement), with only a marginal additional displacement of particles to the left. This also highlights the asymmetry of the installation process. The last pile to be installed (P4) will be more constrained than the first pushed pile (P1). However, it is interesting to note that the displacement field at the end of the sequence (Figure *7*b) is still fairly symmetrical. Although this can be due to the impose displacement control.

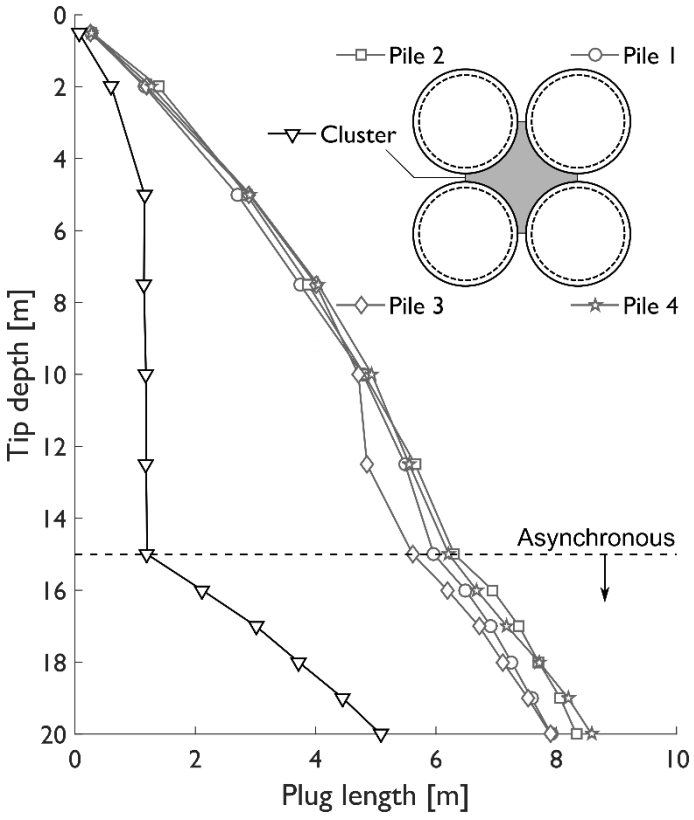

Figure 8 Plugging of the cluster and the individual piles for a displacement-controlled installation

The plugging of the piles was measured internally in the open-ended piles and in the middle of the cluster. The plugging behaviour is important, especially in the middle of the cluster, because the absence of soil in between the piles will inhibit stress redistribution between the different piles. The evolution of the plug length, measured from the base of the piles/cluster, as a function of the tip depth is depicted in Figure 8. This figure shows distinct behaviour between the synchronous and asynchronous installation phases. During the first phase, the inside of the cluster plugged very early and the plug length is equal to 1.2m. This length increases rapidly when the asynchronous installation sequence starts (15m depth). On the contrary, the open-ended piles are only partially plugged. At the end of the simulation, less than half of the pile length was filled with particles.

However, the ratio of the smallest dimension of the cluster inside space (=$0.5D_c$) to the largest particle diameter (d_{100}) is equal to 2. The ratio of the inside pile diameter to d_{100} is equal to 3.8. There is no guidance available in the DEM literature on the minimum value of this ratio to ensure there is no particle scale effect on plugging behaviour. It could be expected that larger particles can create premature plugging of the cluster or the pile, similarly to the effects coarse gravel, cobbles or boulders could have on piles in the

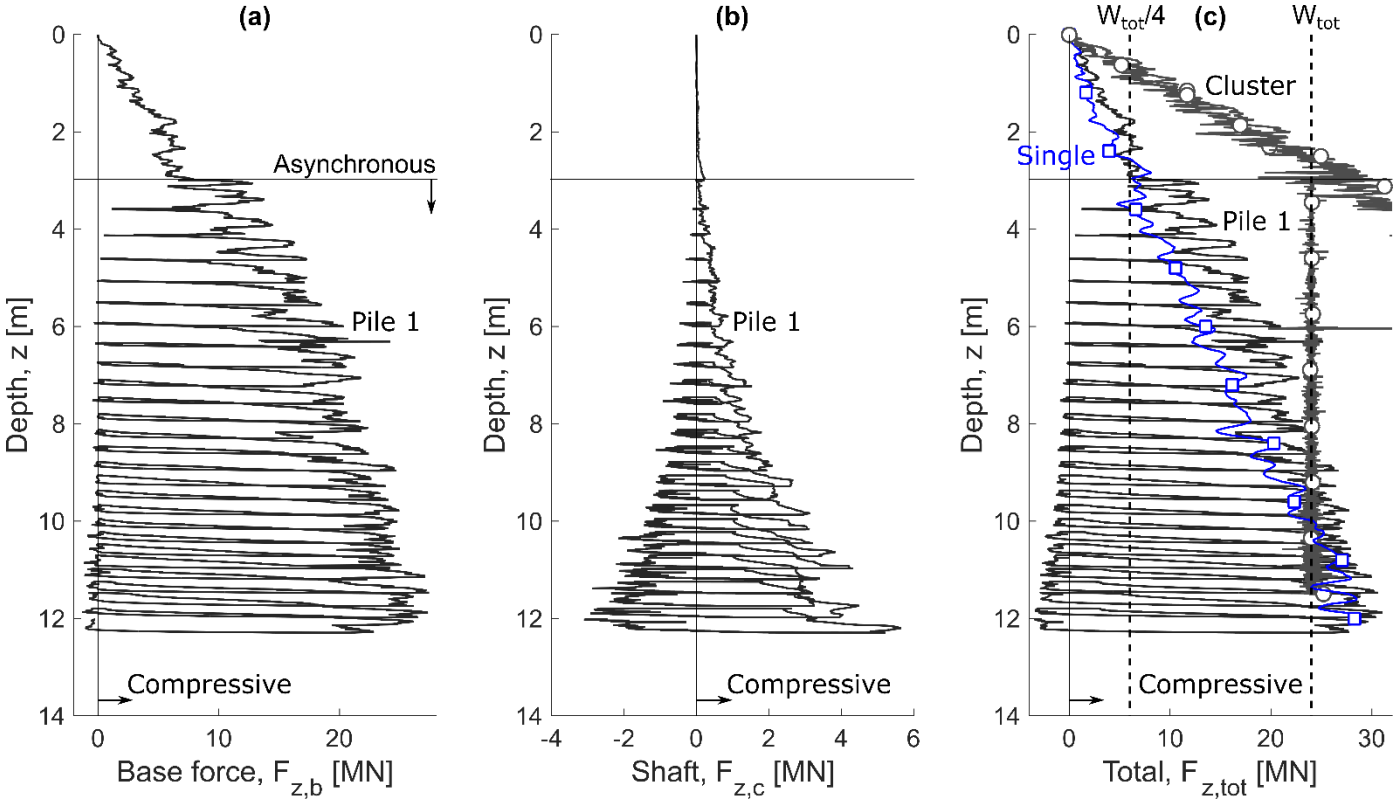

Figure 9 Comparison of the force acting on pile 1 (total, base and shaft) and the total force acting on the cluster during the load-controlled installation with the total force for a single pile

field. Further simulations with smaller particles or experiments are necessary to verify the observed cluster plugging behaviour.

4 FORCE-CONTROLLED

The basic mechanisms of the push-in method have been detailed in the previous section. However, the necessary forces measured largely exceed what is typically available in the field. A more realistic installation process was then simulated.

The synchronous phase took place between 0-3m depth. At approximately 3m depth, the force necessary to jack all the piles together (penetration resistance) is equal to the total dead weight of the piles (4 times W_{piles} = 4MN) and the installation tool (W_{tool} = 20MN here).

During the force-controlled asynchronous installation phase, each pile is pushed downwards by a 0.5m stroke in the same sequence as previously. However, while one pile is pushed downwards (the active pile), the other piles are moved upwards together to mobilise some tensile capacity along their shaft. Therefore, throughout the asynchronous phase, the following equilibrium condition must be met

$$\sum_{i=1}^{4} F_{z,i} = W_{tool} + 4W_{pile} = W_{tot} \quad (3)$$

where $F_{z,i}$ is the total vertical force acting at the top of each pile (positive in compression) and W_{tot} is the total dead weight. In the DEM, this condition is ensured by a servo controlling the vertical uplift displacement of the reaction piles. Each pile is successively active in compression, then becomes a reaction pile. One sequence of cluster installation consists of a series of strokes applied to piles P1, P3, P2 and finally P4.

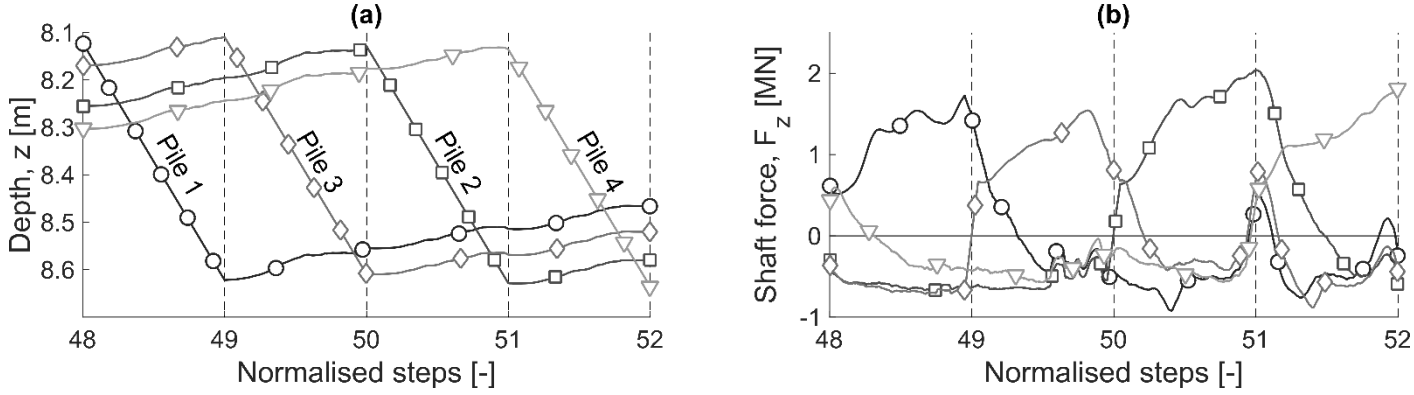

Figure 10 Zoom-in on one asynchronous installation sequence for closed-ended piles, force-controlled installation

The base, shaft and total vertical force related to pile P1 are depicted in Figure *9*. Figure *9*c shows that the total force acting on the cluster is approximately equal to the total weight at a depth equal to 3m. This was selected as the maximum penetration depth during the synchronous phase. Below this depth, the total force acting on the cluster is constant and equal to the dead weight.

Figure *9*c also shows that the total force necessary to install pile P1 (as part of a cluster) is larger than the total force necessary if a single pile was installed. However, the extra force required is lower than in the previous displacement-controlled case. At greater depths (11-12m), the force necessary to install one pile in the cluster tends to that necessary for a single pile.

In the force-controlled simulations, the reaction piles are moved upwards, rather than being fixed (displacement-controlled). This upwards movement mobilises the tensile capacity of the shaft, but will also reduce the constraining effect of the reaction piles on the active pile penetration failure mechanism. This explains why the vertical total force per pile is not that different from the force necessary to penetrate a single pile.

One of the main mechanisms of the load-displacement installation is the compressive load redistribution between the piles. At the end of the synchronous phase (3m depth), the total weight of the tool and piles is equally distributed between the piles. When the reaction piles are moved upwards, the vertical total force is reduced and the piles can even be loaded in tension along the shaft (Figure *9*b). Therefore, the resulting compressive force (W_{tot}) is only balanced by the active pile. This happens between 3-10m depths in Figure *9*c. Beyond this depth, the necessary installation force is greater than the dead weight W_{tot}. Tension must be mobilised in the reaction piles to maintain the equilibrium. It can be observed that as the depth increases, the base force in the reaction pile tends to zero (Figure *9*a) and the shaft is mobilised in tension (Figure *9*b). At some point, the tensile capacity mobilised in all three reaction piles is not sufficient to overcome the necessary penetration force and the installation hits refusal at approximately 12m depth. The refusal depth depends on the soil conditions, the pile and cluster geometries. Further work is necessary to optimise those parameters to maximise the penetration depth.

The capacity of the cluster at a depth of 12m could be approximated from Figure *4*. Indeed, the compressive capacity can be assumed as the force necessary to install the cluster in a synchronous manner at 12m depth. This force is equal to 120MN approximately. Therefore, it can be concluded that a 20MN weight tool can install a cluster whose capacity is 6 times its own weight.

The corollary effect of the reaction pile uplift during the installation, is that the average cluster penetration displacement reached after each sequence of four strokes is lower than the stroke applied to each individual pile (Figure *11*a). As the cluster penetrates further down, a greater uplift displacement is necessary to mobilise the full friction along the reaction pile shaft, reducing the efficiency of the installation. Consequently, more strokes will be necessary to achieve the target depth.

Figure *11* shows the displacement over one installation sequence (four strokes) of each pile, as a function of the average cluster depth. In this example, the displacement of piles P3 and P4 is significantly lower than the two other piles, beyond a depth of approximately 9m. Consequently, a differential penetration accumulates between the piles. Although this does not pose any problem for the DEM simulation, this differential installation must be continuously corrected in the field, as the installation tool cannot accommodate such a large difference.

5 CONCLUSIONS

This paper presents numerical simulations of the installation of a novel silent piling concept. This concept uses a cluster of four closely spaced piles which are jacked asynchronously. During one sequence of installation, each pile is successively pushed downwards of a stroke equal to 0.5m. The dead weight of the installation tool and the piles, together with the tensile capacity of the three remaining piles are used as a reaction for the necessary jacking force.

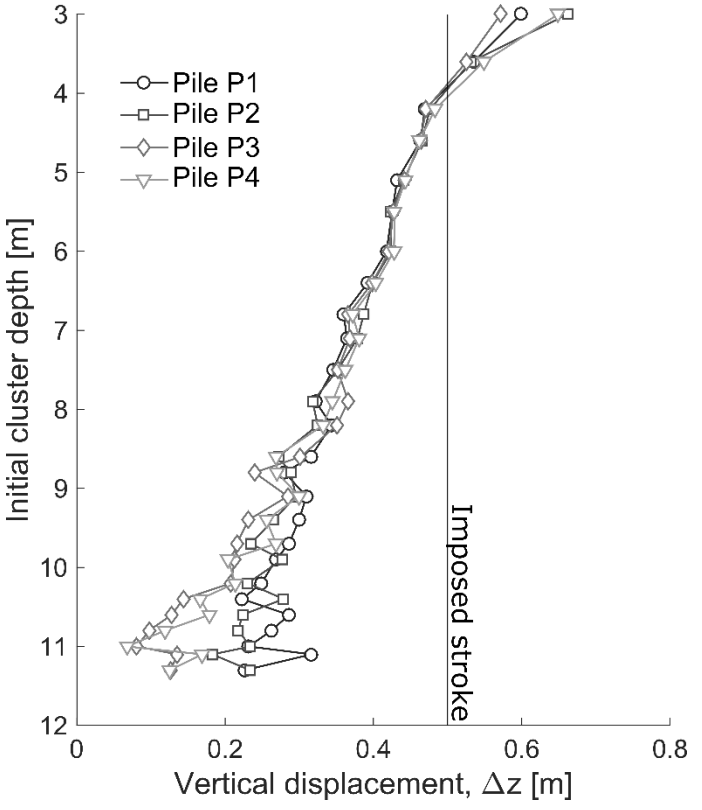

Figure 11 Displacement of each individual pile at the end of one cycle (4 strokes) of load-controlled installation

The DEM technique enables an insightful investigation of the installation mechanisms, as both macroscopic forces and microscopic observations are possible. It also permits simulation of the large soil displacement inherent in the pile penetration process.

The simulations compared synchronous (all piles together) and asynchronous (successive jacking of individual piles by 0.5m strokes) installations. It was shown that the asynchronous installation under a constant dead weight enables the piles to reach a much greater depth (12m) than the synchronous installation (3m). This is due to the redistribution of the dead weight between the four piles for synchronous loading, to a single pile during the asynchronous installation.

The force necessary to install a pile as a part of a cluster, was shown to be greater than the force necessary to install a single pile. This is due to the restraining effect of adjacent piles on the penetration failure mechanism. The DEM particle movements are laterally limited by the adjacent piles. This constraint is progressively reduced as the adjacent piles are moved upwards to provide tensile reaction for the installation tool.

A vertical upwards displacement is necessary to mobilise the tension along the reaction pile. As a consequence, the net cluster penetration displacement for a cycle of four strokes (one for each pile) is lower than the displacement imposed on each individual pile. This loss of efficiency increases with depth. Beyond a certain depth, the efficiency tends to zero and/or the tensile capacity of the reaction pile is insufficient to push the active pile further.

This work has shown that the group push-in pile concept is worthy of further investigation. The numerical simulations showed that a cluster of piles can be jacked 'silently' and indicated that a capacity equal to six times the tool weight necessary for installation. Further work is necessary to assess the installations requirements as a function of the pile spacing, predict the tensile capacity of the pile with depth or optimise the pile control to minimise the loss of efficiency for each asynchronous cycle.

6 REFERENCES

Bailey, H., Senior, B., Simmons, D., Rusin, J., Picken, G. & Thompson, P. M. (2010) 'Assessing underwater noise levels during pile-driving at an offshore windfarm and its potential effects on marine mammals', *Marine Pollution Bulletin*, 60(6), pp. 888–897. doi: 10.1016/j.marpolbul.2010.01.003.

Ciantia, M. O., Arroyo, M., Butlanska, J. & Gens, A. (2016) 'DEM modelling of cone penetration tests in a double-porosity crushable granular material', *Computers and Geotechnics*, 73, pp. 109–127. doi: 10.1016/j.compgeo.2015.12.001.

Ciantia, M. O., Arroyo, M., O'Sullivan, C., Gens, A. & Liu, T. (2019a) 'Grading evolution and critical state in a discrete numerical model of Fontainebleau sand', *Geotechnique*, 69(1), pp. 1–15. doi: 10.1680/jgeot.17.P.023.

Ciantia, M. O., Boschi, K., Shire, T. & Emam, S. (2018) 'Numerical techniques for fast generation of large discrete-element models', *Proceedings of the Institution of Civil Engineers - Engineering and Computational Mechanics*, 171(4), pp. 147–161. doi: 10.1680/jencm.18.00025.

Ciantia, M. O., O'Sullivan, C. & Jardine, R. J. (2019b) 'Pile penetration in crushable soils : Insights from micromechanical modelling', in *Proceedings of the XVII ECSMGE-2019*. Reykjavik, Iceland, Iceland, pp. 298–317. doi: 10.32075/17ECSMGE-2019-1111.

Evans, T. M. & Valdes, J. R. (2011) 'The microstructure of particulate mixtures in one-dimensional compression : numerical studies', pp. 657–669. doi: 10.1007/s10035-011-0278-z.

Itasca Consulting Group (2019) 'PFC3D 6.17'.

Janda, A. & Ooi, J. Y. (2016) 'DEM modeling of cone penetration and unconfined compression in cohesive solids', *Powder Technology*, 293, pp. 60–68. doi: 10.1016/j.powtec.2015.05.034.

Khoubani, A. & Evans, T. M. (2018) 'An efficient flexible membrane boundary condition for DEM simulation of axisymmetric element tests', *International Journal for Numerical and Analytical Methods in Geomechanics*, 42(4), pp. 694–715. doi: 10.1002/nag.2762.

Koschinski, S. & Lüdemann, K. (2013) *Development of Noise Mitigation Measures in Offshore Wind Farm Construction 2013, Report commissioned by the Federal Agency for Nature Conservation (Germany)*.

Lauder, K. (2010) *The performance of pipeline ploughs*. University of Dundee, UK.

Li, Z., Haigh, S. K. & Bolton, M. D. (2010) 'Centrifuge modelling of mono-pile under cyclic lateral loads', *Proceedings of the 7th International Conference on Physical Modelling in Geotechnics*, 2, pp. 965–970. doi: 10.1680/ijpmg.2010.10.2.47.

Liu, J., Ph, D., Duan, N., Ph, D., Cui, L., Ph, D., *et al.* (2019) 'DEM investigation of installation responses of jacked open-ended piles', *Acta Geotechnica*, 14(6), pp. 1805–1819. doi: 10.1007/s11440-019-00817-7.

O'Sullivan, C. (2011) *Particulate Discrete Element Modelling, Particulate Discrete Element Modelling*. Spon Press. doi: 10.1201/9781482266498.

Sharif, Y. U., Brown, M. J., Ciantia, M. O., Cerfontaine, B., Davidson, C., Knappett, J., *et al.* (2020) 'Using DEM to create a CPT based method to estimate the installation requirements of rotaty installed piles in sand', *(in press) Canadian Geotechnical Journal*. doi: 10.1139/cgj-2020-0017.

Shire, T., Hanley, K. J. & Stratford, K. (2020) 'DEM simulations of polydisperse media: efficient contact detection applied to investigate the quasi-static limit', *Computational Particle Mechanics*. doi: 10.1007/s40571-020-00361-2.

White, D., Finlay, T., Bolton, M. & Bearss, G. (2002) 'Press-in piling: Ground vibration and noise during pile installation', in *Deep Foundations 2002: An International Perspective on Theory, Design, Construction, and Performance*, pp. 363–371.

Zhang, N., Arroyo, M., Ciantia, M. O., Gens, A. &

Butlanska, J. (2019) ‘Standard penetration testing in a virtual calibration chamber’, *Computers and Geotechnics*, 111(March), pp. 277–289. doi: 10.1016/j.compgeo.2019.03.021.

Zhang, Z. & Wang, Y. H. (2015) ‘Three-dimensional DEM simulations of monotonic jacking in sand’, *Granular Matter*, 17(3), pp. 359–376. doi: 10.1007/s10035-015-0562-4.